A statistical study of electron acceleration behind the dipolarization fronts in the magnetotail

MingYu Wu,[1,2] QuanMing Lu,[1] Martin Volwerk,[3] Zoltán Vörös,[3] TieLong Zhang,[1,3] LiCan Shan,[1] and Can Huang [1]

Received 9 February 2013; revised 26 June 2013; accepted 17 July 2013; published 8 August 2013.

[1] We investigate the electron acceleration behind dipolarization fronts (DFs) in the magnetotail from $-25\ R_E$ to $-10\ R_E$ through the examination of the energetic electron energy flux (>30 keV) with the observations from Time History of Events and Macroscale Interactions during Substorms (THEMIS). Statistical results of 133 DF events are presented based on the data set from January to April of the years 2008 and 2009. As the DFs propagate earthward, the acceleration of energetic electrons behind the DFs is found to take place over several R_E along the tail. The increase in energetic electron energy flux can reach 2–4 orders of magnitude. The dominant acceleration mechanisms are different in the midtail ($X_{GSM} \leq -15\ R_E$) and the near-Earth region ($-15 < X_{GSM} \leq -10\ R_E$). In the midtail, the majority of DF events show that the dominant electron acceleration mechanism is betatron acceleration. In the near-Earth region, betatron acceleration is dominant in ~46% DF events while Fermi acceleration is dominant in ~39% DF events.

Citation: Wu, M. Y., Q. M. Lu, M. Volwerk, Z. Vörös, T. L. Zhang, L. C. Shan, and C. Huang (2013), A statistical study of electron acceleration behind the dipolarization fronts in the magnetotail, *J. Geophys. Res. Space Physics*, *118*, 4804–4810, doi:10.1002/jgra.50456.

1. Introduction

[2] Dipolarization fronts (DFs) are characterized by sharp enhancements of the northward magnetic field B_z in the plasma sheet of the magnetotail [*Nakamura et al*., 2002]. Observations by Geotail, Cluster, and Time History of Events and Macroscale Interactions (THEMIS) have shown that the sharp B_z enhancements of the DFs are typically preceded by a minor B_z dip [*Ohtani et al*., 2004; *Runov et al*., 2009; *Schmid et al*., 2011]. These DFs are tangential discontinuities [*Schmid et al*., 2011] and mostly observed to be associated with busty bulk flows (BBFs) [*Angelopoulos et al*., 1994]. As a boundary with a typical scale of about 1.8 ion inertial lengths, they have always been suggested to separate hot and tenuous BBF plasma from the ambient cold and dense plasma sheet [*Runov et al*., 2011]. Both kinetic simulations and the observations have pointed out that DFs can be produced during magnetic reconnection [*Sitnov et al*., 2009; *Sitnov et al*., 2013; *Runov et al*., 2012]. After the generation, they can propagate earthward from the midtail to the near-Earth region in a few minutes [*Runov et al*., 2009].

[3] DFs have been suggested to be associated with aurorae and substorms [*Baumjohann et al*., 1999; *Volwerk et al*., 2008]. The energetic electrons (about 30–200 keV) can be accelerated within the DFs during substorm [*Birn et al*., 2004; *Ashour-Abdalla et al*., 2011]. Based on the THEMIS measurements of six events, *Runov et al*. [2011] indicated that the DFs are always accompanied with large variations of the energetic electron flux (30–200 keV) and electron temperature. In principle, the electron acceleration and energetic electron flux increases are consistent with betatron acceleration and Fermi acceleration in the magnetotail [*Smets et al*., 1999; *Birn et al*., 2004; *Wu et al*., 2006]. The enhancements of the energetic electron flux at large pitch angles (around 90°) are caused by betatron acceleration due to magnetic field compression as DFs propagate earthward, and at small pitch angles (around 0° or 180°) by Fermi acceleration due to a decrease of the distance between mirror points [e.g., *Northrop*, 1963; *Pan et al*., 2012]. These adiabatic acceleration processes can affect the pitch angle distributions of these energetic electrons. The betatron acceleration leads to pancake distributions (peak in pitch angle around 90°) [e.g., *Birn et al*., 2004] while the Fermi acceleration leads to cigar distributions (peak in pitch angle around 0° and 180°) [e.g., *Wu et al*., 2006]. *Fu et al*. [2011] observed cigar distributions inside a decaying flux pileup region and pancake distributions in a growing flux pileup region, which were considered to be caused by Fermi and betatron accelerations, respectively. The statistical results of energetic electrons (>40 keV) has confirmed this suggestion [*Fu et al*., 2012c].

[4] In this paper, based on the observations by the THEMIS Mission, the variations of electron energy flux (>30 keV) associated with the DFs are studied. We investigate

[1]CAS Key Laboratory of Geospace Environment, Department of Geophysics and Planetary Science, University of Science and Technology of China, Hefei, China.
[2]State Key Laboratory of Space Weather, Chinese Academy of Sciences, Beijing, China.
[3]Space Research Institute, Austrian Academy of Sciences, Graz, Austria.

Corresponding author: Q. Lu, CAS Key Laboratory of Geospace Environment, Department of Geophysics and Planetary Science, University of Science and Technology of China, 96 JinZhai Rd., Hefei, Anhui 230026, China. (qmlu@ustc.edu.cn)

2169-9380/13/10.1002/jgra.50456

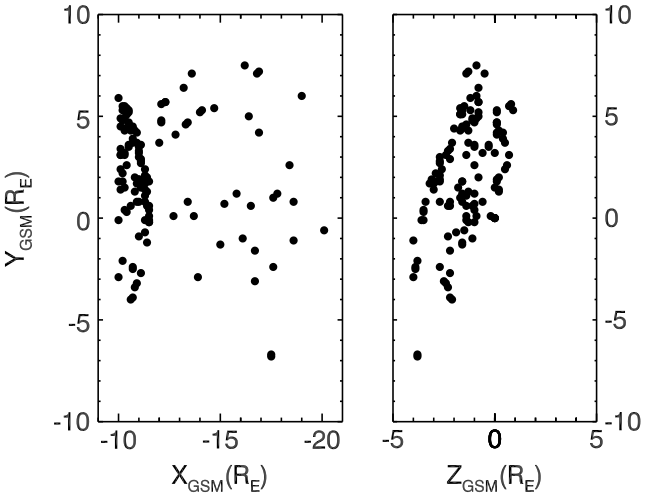

Figure 1. The THEMIS spacecraft positions in the *XY* and *YZ* planes in the GSM coordinate for all the 131 earthward dominate events observed from January to April during the years 2008 and 2009.

the evolution of energetic electrons when DFs propagates from the midtail to the near-Earth region, and try to figure out the role of betatron and Fermi accelerations in the electron energization processes associated with earthward-propagating DFs.

2. Data and Selection Criteria of DF

[5] Each THEMIS probe carries identical instruments. For the DF event selection, we use the 4 Hz magnetic field data obtained by the fluxgate magnetometer [*Auster et al*., 2008], 3 s spin-average plasma data with low energies (less than 30 keV) from the electrostatic analyzers [*McFadden et al*., 2008] and high energies (more than 30 keV) from the Solid State Telescopes (SST) [*Angelopoulos*, 2008]. To survey the DF events in the plasma sheet, we used the data set from January to April of the years 2008 and 2009, while THEMIS had its apogee in the magnetotail.

[6] In our study, the geocentric solar magnetospheric (GSM) coordinate system is used unless noted otherwise. We consider only DFs in the region $-10 \geq X_{GSM} > -25\ R_E$, $|Y_{GSM}| < 10\ R_E$, and $|Z_{GSM}| < 10\ R_E$. In this region, the DF associated with a BBF can be distinguished using the flow velocity, as the DF is a tangential discontinuity. In order to identify DFs, in the magnetic field and plasma data, we use the criteria given by *Schmid et al*. [2011] and use 3 min sliding windows, shifted by 1.5 min. After identifying these events, we select only "steep" DFs. The details of these procedures are given below.

[7] As previous studies [*Schmid et al*., 2011; *Fu et al*., 2012a] have shown, the DF is a special region of dipolarization events and has a typical pulse of several seconds. The DFs can be characterized by the significant increase of B_z. The *Schmid et al*.'s [2011] criteria for identifying the dipolarization events are the following: (a) a large plasma beta (max $(\beta) \geq 0.5$), (b) a large earthward flow velocity ($\max(v_{\perp x}) \geq$ 150 km/s), (c) a finite difference of elevation angle from minimum B_z to maximum B_z ($\theta_1 - \theta_2 \geq 10°$), (d) a large jump of B_z ($\max(B_z) - \min(B_z) \geq 4$ nT), and (e) a large elevation angle of magnetic field ($\max(\theta) \geq 45°$) in each window.

[8] After the identification, we restrict the events with more requirements. First of all, we only choose the events with earthward dominant flow and exclude those events for which the flow turns tailward. We are only interested in "steep" DFs which B_z changes more than 5 nT/s from the minimum to the maximum of B_z. In addition, the events without pitch angle data of energetic electrons (>30 keV) are excluded. Finally, we have found 133 dipolarization front events.

3. Observations

[9] Figure 1 shows the locations of the THEMIS satellites for the 133 dipolarization events in the GSM *XY* and *YZ* planes. The locations of these DFs are distributed in the magnetotail $-10 \geq X_{GSM} > -21\ R_E$ near the center of the plasma sheet. In this figure, we show that there are more DF events in $-10 \geq X_{GSM} > -21\ R_E$ than in other regions. This might be dependent on the characteristics of the spacecraft orbits and the normalized occurrence rate of DFs [*Fu et al*., 2012b].

[10] In this paper, the arrival time of a DF, t_{DF}, is defined by the minimum of B_z that is immediately prior to the sharp enhancement of B_z in the DF region. Figure 2 presents the superposed epoch analysis of B_z for the 133 earthward dominant DF events (black lines) during the time interval from 1 min before to 1 min after t_{DF}. From these 133 events, 22 DF events distributed in $-15 \geq X_{GSM} > -21\ R_E$ are shown in Figure 2a, and 111 DF events distributed in $-10 \geq X_{GSM} > -15\ R_E$ are shown in Figure 2b. The medians (green lines) of the two superposed B_z are also plotted. As in the earlier results, there is a minor decrease before the B_z starts to increase for both median lines. In the region $-15 \geq X_{GSM} > -21\ R_E$, the median value of B_z jumps from 1.3 to 16.0 nT in about 2 s at the DF. However, in the region $-10 \geq X_{GSM} > -15\ R_E$, the decrease in median B_z is more obvious and deeper. The median B_z in Figure 2b falls off faster after the maximum than in Figure 2a. Comparing the median lines of Figures 2a and 2b, we can find that the peak value of B_z at the DF in the region $-10 \geq X_{GSM} > -15\ R_E$ is larger than in the region $-15 \geq X_{GSM} > -21\ R_E$. This can be explained as the result of compression during the DF propagation.

[11] The superposed epoch analysis of the motional electric field, $\mathbf{E} = -\mathbf{V} \times \mathbf{B}$, is shown in Figure 3. Figure 3a shows the three components of the electric field in the region $-15 \geq X_{GSM} > -21\ R_E$ while Figure 3b gives the results in the region $-10 \geq X_{GSM} > -15\ R_E$. The green lines are the medians of the electric field. According to the six median lines, we can find that the *x* and *z* components are negligible while the *y* component increases obviously just behind the DFs. The peak value of E_y which is mainly generated by $V_x B_z$ is 3.3 mV/s in $-15 \geq X_{GSM} > -21\ R_E$. In $-10 \geq X_{GSM} > -15\ R_E$, the peak value of E_y is a little smaller, at 2.8 mV/s.

[12] On 27 February 2009, THEMIS THB (r_B=(−20.1, −0.6, −1.5) R_E), THC (r_C=(−16.7, −1.6, −2.2) R_E), THD (r_D=(−11.1, −1.8, −2.4)R_E), and THE (r_E=(−11.1, −2.8, −2.1) R_E) detected similar earthward-propagating dipolarization fronts [*Runov et al*., 2009]. Because the bursty bulk flows can expand 2–3 R_E in the dawn-dusk direction and 1.5–2 R_E in the north-south direction [*Nakamura et al*., 2004], these dipolarization fronts were possibly in the same

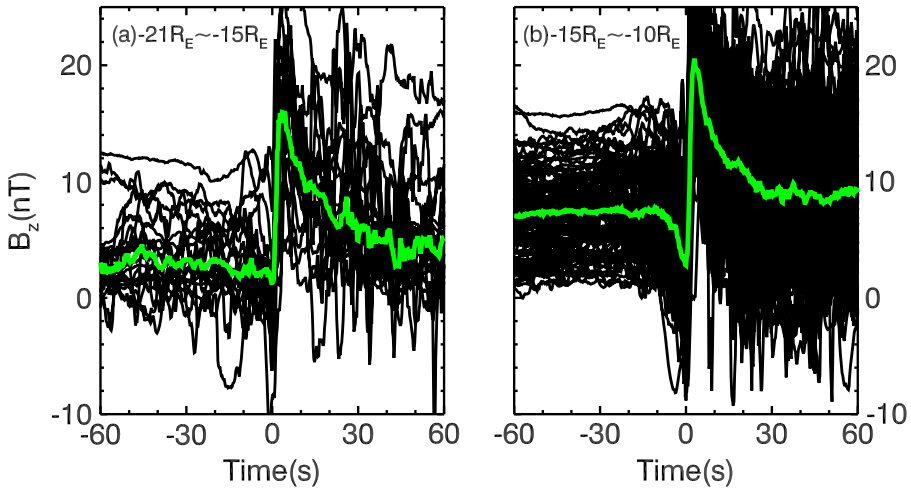

Figure 2. (a) The B_z of the 22 dipolarization fronts (black line) and the median (green line) over these DFs in the region $-15 \geq X_{GSM} > -21\ R_E$. (b) The B_z of the 111 dipolarization fronts (black line) and the median (green line) over these DFs in the region $-10 \geq X_{GSM} > -15\ R_E$.

flow channel. This event can be considered to be a DF observed by multiple spacecraft at different locations in the magnetotail. Figure 4 shows the B_z components and pitch angle distributions within the energy range above 30 keV obtained by SST instruments. The first panel shows the B_z observed by four spacecraft. Each dashed vertical line marks the arrival time t_{DF} of the DF. The other four panels give the pitch angle distributions. The two outermost spacecraft THB (at $X_{GSM} = -20.1\ R_E$) and THC (at $X_{GSM} = -16.7\ R_E$) observed pancake distributions of the energetic electrons (>30 keV) behind the DF, while

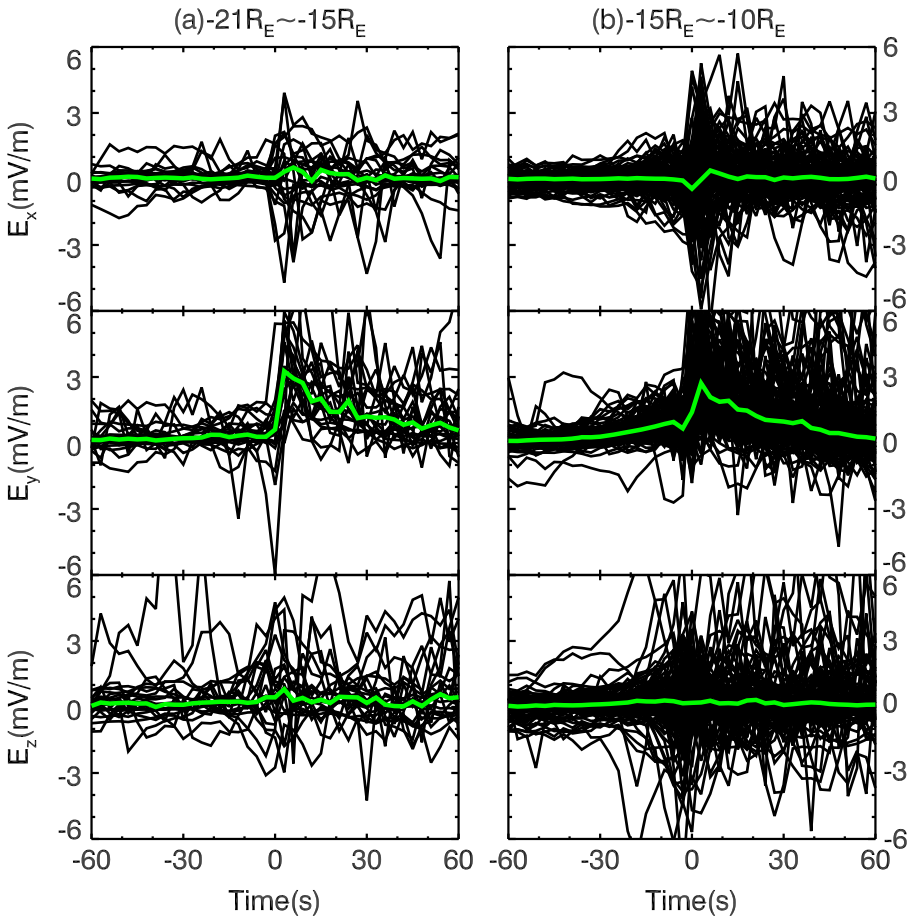

Figure 3. (a) The (top) x, (middle) y, and (bottom) z of the electric field which is calculated by $\mathbf{E} = -\mathbf{V} \times \mathbf{B}$ in the region $-15 \geq X_{GSM} > -21\ R_E$. (b) The electric field in the region $-10 \geq X_{GSM} > -15\ R_E$. The green lines are the median values.

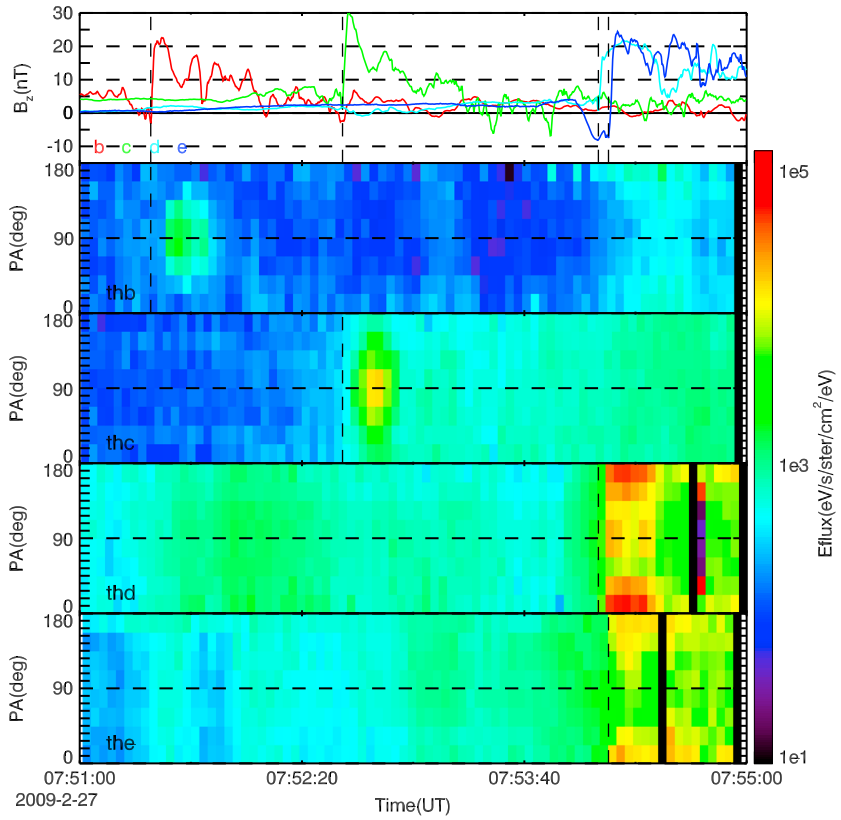

Figure 4. The first panel shows the B_z components observed by THB (red), THC (green), THD (cyan), and THE (blue). The other four panels show the pitch angle distributions of energetic electrons (>30keV) energy flux (Eflux). The dashed vertical lines indicate the arrival time of the DF.

the THD and THE (both at about $X_{GSM} = -11.1\ R_E$) observed cigar distributions behind the DF. This result reveals that betatron acceleration is dominant in the midtail while Fermi acceleration is dominant in the near-Earth region in this event. We can also find that the maximum of the energetic electron energy flux behind the DF has a large increase from $X_{GSM} = -20.1\ R_E$ (THB) to $X_{GSM} = -16.7\ R_E$ (THC), also an increase from $X_{GSM} = -16.7\ R_E$ (THC) to $X_{GSM} = -11.1\ R_E$ (THD and THE). This event shows the large increase of electron energy flux and the change of the dominant acceleration mechanism during the propagation of a DF. A statistical study is used below to check whether these two features are existing during the propagation of most DFs.

[13] The variations of energetic electron energy flux in the quiet plasma sheet is negligible before a DF, whereas the energetic electron energy flux after the steep DF changes quickly and can reach the maximum in several seconds [*Runov et al.*, 2011]. So in this paper, the 30 s average of the energetic electron flux before t_{DF} is F_{before}, and the maximum of the energetic electron flux from t_{DF} to t_{DF} +10 s is F_{DF}. Out of these 133 events, there are three categories of DFs, which depend on the change of the energetic electron flux (>30 keV): (a) increase type whose $F_{DF}/F_{before} \geq 1.1$; (b) decrease type whose $F_{DF}/F_{before} \leq 0.9$; (c) steady type whose $0.9 < F_{DF}/F_{before} < 1.1$. In our study, there are 88 increase type DFs, 32 decrease type DFs, and 13 steady type cases. We also investigate the pitch angle distribution of the energetic electron flux and find that the distributions before t_{DF} and after t_{DF} are quite different for almost all the increase type and decrease type DFs. For example, in Figure 4, the energetic electron distributions just behind the DF are pancake or cigar distributions. However, the energetic electrons are nearly isotropic in the quiet plasma sheet. In this paper, we are only focusing on the electron acceleration behind the DFs, so in the following, we examine the 88 increase type DF events that took place close to the neutral sheet. The event shown in Figure 4 is also an increase type DF. Figure 5 shows the relation between F_{DF} and the

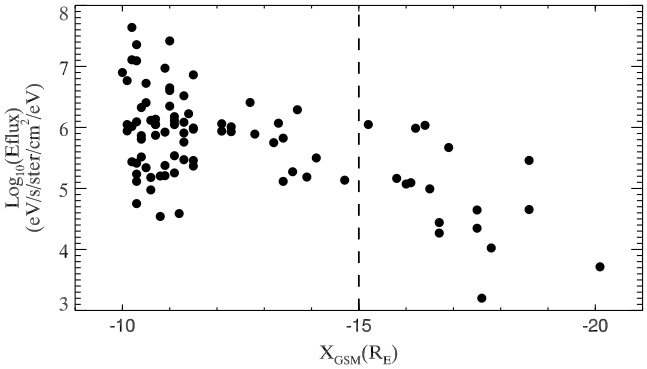

Figure 5. The relationship between the x component of spacecraft location and the maximum value of the energetic electron (>30 keV) energy flux (Eflux) behind the DF in all the increase type DF events observed from January to April of the years 2008 and 2009 by the THEMIS mission.

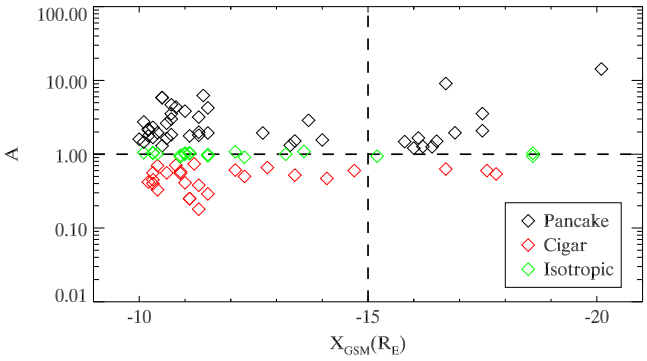

Figure 6. The relationship between the x component of the spacecraft location and the anisotropy factor $A = F_{\perp}/F_{\parallel}$. Different colors represent different pitch angle distributions.

locations of spacecraft of all 88 increase type events. In Figure 5, we can find that the maximum of the energetic electron flux (>30 keV) behind the DFs increases from the midtail to the near-Earth region continuously. The increase in electron energy flux can even reach 2–4 orders of magnitude. Therefore, the acceleration associated with the DFs is very important and effective. It can also be seen in Figure 5 that the maximum of the energetic electron flux increases rapidly from the midtail to ~ -15 R_E. Then, the flux still increases gradually from ~ -15 R_E to ~ -10 R_E, but less rapidly. As shown in Figure 3, the E_y in $-15 \geq X_{GSM} > -21$ R_E is a little stronger than in $-10 \geq X_{GSM} > -15$ R_E. This indicates that there are probably different dominant acceleration mechanisms in these two regions. Therefore, we divide the magnetotail into two parts: one from -25 R_E to -15 R_E, and the other from -15 R_E to -10 R_E.

[14] The pitch angle distribution of energetic electrons can give us more information on the mechanism of electron acceleration. The local compression of the magnetic field leads to betatron acceleration and the electrons obtain a pancake distribution, while the shortening of magnetic flux leads to the Fermi acceleration and the electrons obtain a cigar distribution [*Smets et al.*, 1999; *Birn et al.*, 2004; *Wu et al.*, 2006; *Fu et al.*, 2011]. We examine the pitch angle

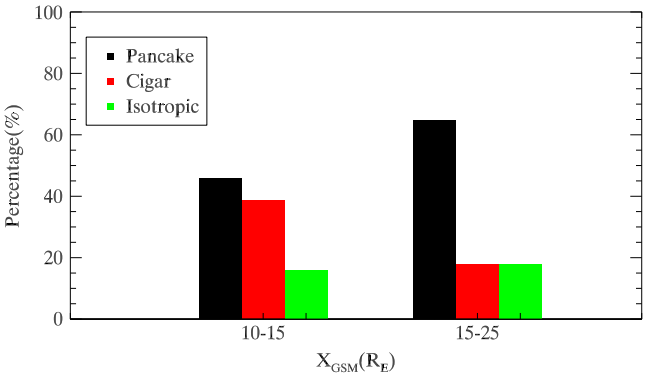

Figure 7. The histogram of percentage of the three distributions for group 10–15 and group 15–25. The pancake distribution is marked by black, the cigar distribution is marked by red, and the isotropic distribution is marked by green. The vertical axis shows the percentage normalized by the total number of each group.

distribution of energetic electrons behind the DFs (from t_{DF} to $t_{DF}+10$ s) for all increase type cases. The perpendicular component of energetic electron energy flux ($F_{\perp}$) is calculated from the average electron energy flux at pitch angles between 75° and 105°, while the cigar component $F_{\parallel}$ is calculated from the average electron energy flux between parallel component (0°–20°) and antiparallel component (160°–180°). The anisotropy factor can be defined as $A = F_{\perp}/F_{\parallel}$. In this paper, the pitch angle distributions are roughly divided into three categories: the isotropic distribution is $0.9 < A < 1.1$, the pancake distribution is $A \geq 1.1$, and the cigar distribution is $A \leq 0.9$. Figure 6 shows the relation of the anisotropy factor A to the x component of the spacecraft location for all 88 increase type DF events (in these events, there is only one event which has no data for $F_{||}$). The maximum and minimum of A can reach ~10 and ~0.1, respectively. However, most of points are in the range [0.3, 4], which is consistent with the results of Cluster observation [*Fu et al.*, 2012c]. From ~ -25 R_E to ~ -15 R_E, 11 events have pancake distributions, 3 events have cigar distributions, and 3 events have isotropic distributions. From ~ -15 R_E to ~ -10 R_E, the number of the pancake, cigar, and isotropic distributions is 32, 27, and 11, respectively. For comparison, we normalized the number of the three distributions by the total number of all events in the region -25 R_E to -15 R_E and -15 R_E to -10 R_E, respectively. Figure 7 shows the percentage of the three distributions in the two regions. Black represents the pancake distribution, red represents the cigar distribution, and green represents the isotropic distribution. In the region -25 R_E to -15 R_E, betatron acceleration is prominent in 65% DF events. It seems that betatron acceleration caused by compression of the magnetic field is dominant in the midtail. However, in the region -15 R_E to -10 R_E, the percentage of pancake distribution (46%) and cigar distribution (39%) are nearly the same, which leads us to conclude that both betatron and Fermi accelerations can work in this region.

4. Discussion and Conclusions

[15] Based on the 133 earthward-propagating DF events, we examine the acceleration mechanisms of the energetic electrons behind the DFs from $X_{GSM} \sim -25$ R_E to ~ -10 R_E. In these 133 events, there are 18 DFs which are possibly observed by multiple spacecraft in the different locations of the magnetotail. The energetic electrons behind these DFs have different distributions or different energy fluxes at different locations. One of them, the event observed by 27 February 2009 has been shown as an example. A conclusion can be inferred from the observations of this event: During the propagation of a DF from ~20 R_E to ~ -11 R_E, betatron acceleration of electrons is dominant in the midtail while Fermi acceleration becomes important in the near-Earth region. In this event, the flux at ~ -11 R_E is higher than at ~ -17 R_E, and the flux at ~ -17 R_E is much higher than at ~ -20 R_E.

[16] The event observed by 27 February 2009 is an increase type DF. We investigate the 88 increase type DFs and study electron acceleration behind the DFs. The DFs can be assumed to be quasi-steady and lead a sustained acceleration for several R_E during the propagation. Electrons can be efficiently accelerated behind the DFs. The energetic electron energy flux can be enhanced about 2–4 orders of magnitude from

the midtail to the near-Earth region. In our work, the magnetotail is divided into two parts: the midtail region (from $-25\ R_E$ to $-15\ R_E$) and the near-Earth region (from $-15\ R_E$ to $-10\ R_E$). The maximum of B_z at the DF in the midtail region is smaller than that in the near-Earth region, while the y component of motional electric field has larger values in the midtail region than in the near-Earth region. In the two regions, we find that the pitch angle distribution of energetic electrons is mainly a pancake distribution in the midtail region. However, in the near-Earth region, the percentage of cigar distributions is ~39% and of pancake distributions is ~46%. This result reveals that the dominant acceleration mechanisms of energetic electrons behind DFs are different during the time evolution of the DFs. Here we give a possible explanation: after the DF and its accompanying high-speed plasma flow is generated through magnetic reconnection in the midtail, it propagates toward the Earth. In the midtail, the electric field $E_y \approx V_x B_z$ is larger than in the near-Earth region for a smaller B_z . This means that in the midtail, the speed of the earthward flows is much higher than closer to Earth (see, for flow braking in the tail, e.g., *Baumjohann* [2002] and *Panov et al*. [2010]). The high-speed flows are expected to efficiently compress the magnetic field [e.g., *Ohtani et al*., 2004]. The more efficient compression of the local magnetic field in this region makes betatron acceleration dominant as compared to near-Earth region. This could be an important reason for why the energetic electron flux increases more rapidly in the midtail. As the DF propagates to the Earth, the flows become weaker and weaker, and Fermi acceleration becomes dominant in some DF events due to the length shortening of the flux tubes. So the percentage of cigar distributions in the near-Earth region is much higher than in the midtail (~18% in our study).

[17] In the magnetotail, magnetic reconnection is also an effective acceleration mechanism [e.g., *Øieroset et al*., 2002; *Chen et al*., 2007; *Wang et al*., 2010], and the reconnection electric field can accelerate the electrons [e.g., *Hoshino et al*., 2001; *Pritchett*, 2006; *Huang et al*., 2010]. However, in all of our DF events, the X line is not observed by the THEMIS Mission, and it should be far away from the DFs. Therefore, the local acceleration through magnetic reconnection can be excluded in our studies. Some nonadiabatic effects such as wave-particle interactions (for example, with whistler waves) [*Khotyaintsev et al*., 2011; *Deng et al*., 2010], may also affect the dynamics of the energetic electrons. The DF events influenced by wave-particle interactions will be studied in future work.

[18] **Acknowledgments.** We acknowledge NASA contract NAS502099 for use of data from the THEMIS Mission. This research was supported by Ocean Public Welfare Scientific Research Project, State Oceanic Administration People's Republic of China (201005017), the Specialized Research Fund for State Key Laboratories, CAS Key Research Program KZZD-EW-01, the 973 Program (2012CB825602), and the National Science Foundation of China, grants 41174124, 41274144, 40931053, and 41121003. The work by Zoltán Vörös was supported by the Austrian Wissenschaftsfonds FWF under grant P24740-N27.

[19] Masaki Fujimoto thanks the reviewers for their assistance in evaluating this paper.

References

Angelopoulos, V. (2008), The THEMIS mission, *Space Sci. Rev.*, *141*, 5–34.

Angelopoulos, V., C. F. Kennel, F. V. Coroniti, R. Pellat, M. G. Kivelson, R. J. Walker, C. T. Russell, W. Baumjohann, W. C. Feldman, and J. T. Gosling (1994), Statistical characteristics of bursty bulk flow events, *J. Geophys. Res.*, *99*, 21,257–21,280.

Ashour-Abdalla, M., M. El-Alaoui, M. L. Goldstein, M. Zhou, D. Schriver, R. Richard, R. Walker, M. G. Kivelson, and K. Hwang (2011), Observations and simulations of non-local acceleration of electrons in magnetotail magnetic reconnection events, *Nat. Phys.*, *7*, 360–365, doi:10.1038/nphys1903.

Auster, H. U., et al. (2008), The THEMIS fluxgate magnetometer, *Space Sci. Rev.*, *141*, 235–264, doi:10.1007/s11214-008-9365-9.

Baumjohann, W. (2002), Modes of convection in the magnetotail, *Phys. Plasmas*, *9*, 3665–3667, doi:10.1063/1.1499116.

Baumjohann, W., M. Hesse, S. Kokubun, T. Mukai, T. Nagai, and A. A. Petrukovich (1999), Substorm dipolarization and recovery, *J. Geophys. Res.*, *104*(A11), 24,995–25,000, doi:10.1029/1999JA900282.

Birn, J., M. F. Thomsen, and M. Hesse (2004), Electron acceleration in the dynamic magnetotail: Test particle orbits in three-dimensional magneto-hydrodynamic simulation fields, *Phys. Plasmas*, *11*, 1825–1833, doi:10.1063/1.1704641.

Chen, L. J., et al. (2007), Observation of energetic electrons within magnetic islands, *Nat. Phys.*, *4*(1), 19–23, doi:10.1038/nphys777.

Deng, X., M. Ashour-Abdalla, M. Zhou, R. Walker, M. El-Alaoui, V. Angelopoulos, R. E. Ergun, and D. Schriver (2010), Wave and particle characteristics of earthward electron injections associated with dipolarization fronts, *J. Geophys. Res.*, *115*, A09225, doi:10.1029/2009JA015107.

Fu, H. S., Y. V. Khotyaintsev, M. André, and A. Vaivads (2011), Fermi and betatron acceleration of suprathermal electrons behind dipolarization fronts, *Geophys. Res. Lett.*, *38*, L16104, doi:10.1029/2011GL048528.

Fu, H. S., Y. V. Khotyaintsev, A. Vaivads, M. André, and S. Y. Huang (2012a), Electric structure of dipolarization front at sub-proton scale, *Geophys. Res. Lett.*, *39*, L06105, doi:10.1029/2012GL051274.

Fu, H. S., Y. V. Khotyaintsev, A. Vaivads, M. André, and S. Y. Huang (2012b), Occurrence rate of earthward-propagating dipolarization fronts, *Geophys. Res. Lett.*, *39*, L10101, doi:10.1029/2012GL051784.

Fu, H. S., Y. V. Khotyaintsev, A. Vaivads, M. André, V. A. Sergeev, S. Y. Huang, E. A. Kronberg, and P. W. Daly (2012c), Pitch angle distribution of suprathermal electrons behind dipolarization fronts: A statistical overview, *J. Geophys. Res.*, *117*, A12221, doi:10.1029/2012JA018141.

Hoshino, M., T. Mukai, T. Terasawa, and I. Shinohara (2001), Suprathermal electron acceleration in magnetic reconnection, *J. Geophys. Res.*, *106*, 4509–4530.

Huang, C., Q. M. Lu, and S. Wang (2010), The mechanisms of electron acceleration in antiparallel and guide field magnetic reconnection, *Phys. Plasmas*, *17*, 072,306, doi:10.1063/1.3457930.

Khotyaintsev, Y. V., C. M. Cully, A. Vaivads, M. André, and C. J. Owen (2011), Plasma jet braking: Energy dissipation and nonadiabatic electrons, *Phys. Rev. Lett.*, *106*, 165,001, doi:10.1103/PhysRevLett.106.165001.

McFadden, J. P., C. W. Carlson, D. Larson, V. Angelopoulos, M. Ludlam, R. Abiad, B. Elliot, P. Turin, and M. Marckwordt (2008), The THEMIS ESA plasma instrument and in-flight calibration, *Space Sci. Rev.*, *141*, 277–302.

Nakamura, R., et al. (2002), Motion of the dipolarization front during a flow burst event observed by Cluster, *Geophys. Res. Lett.*, *29*(20), 1942, doi:10.1029/2002GL015763.

Nakamura, R., et al. (2004), Spatial scale of high-speed flows in the plasma sheet observed by Cluster, *Geophys. Res. Lett.*, *31*, L09804, doi:10.1029/2004GL019558.

Northrop, T. G. (1963), *The Adiabatic Motion of Charged Particles*, Interscience Publishers, New York.

Ohtani, S. I., M. A. Shay, and T. Mukai (2004), Temporal structure of the fast convective flow in the plasma sheet: Comparison between observations and two-fluid simulations, *J. Geophys. Res.*, *109*, A03210, doi:10.1029/2003JA010002.

Øieroset, M., R. P. Lin, T. D. Phan, D. E. Larson, and S. D. Bale (2002), Evidence for electron acceleration up to 300 keV in the magnetic reconnection diffusion region of Earth's magnetotail, *Phys. Rev. Lett.*, *89*, 195,001, doi:10.1103/PhysRevLett.89.195001.

Pan, Q., M. Ashour-Abdalla, M. El-Alaoui, R. J. Walker, and M. L. Goldstein (2012), Adiabatic acceleration of suprathermal electrons associated with dipolarization fronts, *J. Geophys. Res.*, *117*, A12224, doi:10.1029/2012JA018156.

Panov, E. V., et al. (2010), Plasma sheet thickness during a bursty bulk flow reversal, *J. Geophys. Res.*, *115*, A05213, doi:10.1029/2009JA014743.

Pritchett, P. L. (2006), Relativistic electron production during guide field magnetic reconnection, *J. Geophys. Res.*, *111*, A10212, doi:10.1029/2006JA011793.

Runov, A., V. Angelopoulos, M. I. Sitnov, V. A. Sergeev, J. Bonnell, J. P. McFadden, D. Larson, K. Glassmeier, and U. Auster (2009), THEMIS observations of an earthward-propagating dipolarization front, *Geophys. Res. Lett.*, *36*, L14106, doi:10.1029/2009GL038980.

Runov, A., V. Angelopoulos, X.-Z. Zhou, X.-J. Zhang, S. Li, F. Plaschke, and J. Bonnell (2011), A THEMIS multicase study of dipolarization fronts in the magnetotail plasma sheet, *J. Geophys. Res.*, *116*, A05216, doi:10.1029/2010JA016316.

Runov, A., V. Angelopoulos, and X.-Z. Zhou (2012), Multipoint observations of dipolarization front formation by magnetotail reconnection, *J. Geophys. Res.*, *117*, A05230, doi:10.1029/2011JA017361.

Schmid, D., M. Volwerk, R. Nakamura, W. Baumjohann, and M. Heyn (2011), A statistical and event study of magnetotail dipolarization fronts, *Ann. Geophys.*, *29*, 1537–1547, doi:10.5194/angeo-29-1537-2011.

Sitnov, M. I., M. Swisdak, and A. V. Divin (2009), Dipolarization fronts as a signature of transient reconnection in the magnetotail, *J. Geophys. Res.*, *114*, A04202, doi:10.1029/2008JA013980.

Sitnov, M. I., N. Buzulukova, M. Swisdak, V. G. Merkin, and T. E. Moore (2013), Spontaneous formation of dipolarization fronts and reconnection onset in the magnetotail, *Geophys. Res. Lett.*, *40*, 22–27, doi:10.1029/2012GL054701.

Smets, R., D. Delcourt, J. A. Sauvaud, and P. Koperski (1999), Electron pitch-angle distributions following the dipolarization phase of a substorm: Interball-Tail observations and modeling, *J. Geophys. Res.*, *104*(A7), 14,571–14,581, doi:10.1029/1998JA900162.

Volwerk, M., et al. (2008), Magnetotail dipolarization and associated current systems observed by Cluster and Double Star, *J. Geophys. Res.*, *113*, A08S90, doi:10.1029/2007JA012729.

Wang, R. S., Q. M. Lu, A. M. Du, and S. Wang (2010), In situ observations of a secondary magnetic island in an ion diffusion region and associated energetic electrons, *Phys. Rev. Lett.*, *104*, doi:10.1103/PhysRevLett.104.175003.

Wu, P., T. A. Fritz, B. Larvaud, and E. Lucek (2006), Substorm associated magnetotail energetic electrons pitch angle evolutions and flow reversals: Cluster observation, *Geophys. Res. Lett.*, *33*, L17101, doi:10.1029/2006GL026595.